Dalton Transactions

ROYAL SOCIETY OF CHEMISTRY

PAPER

View Article Online
View Journal | View Issue

Check for updates

Cite this: *Dalton Trans.*, 2023, **52**, 18513

Trigonal prismatic coordination geometry imparted by a macrocyclic ligand: an approach to large axial magnetic anisotropy for Co(II)†

Eva Zahradníková, [a] Jean-Pascal Sutter, *[b] Petr Halaš [a] and Bohuslav Drahoš *[a]

Received 13th August 2023,
Accepted 13th November 2023

DOI: 10.1039/d3dt02639f

rsc.li/dalton

Large uniaxial magnetic anisotropy, expressed by a negative value of the axial zero-field splitting parameter *D*, has been achieved in a series of trigonal prismatic Co(II) complexes with the general formula [Co(**L**)X]Y, where **L** = 1,5,13,17,22-pentaazatricyclo[15.2.2.17,11]docosa-7,9,11(22)-triene, X = Cl^-(**1a,b**), Br^-(**2**), N_3^-(**3**), NCO^-(**4**), NCS^-(**5**), $NCSe^-$(**6**), and Y = Cl^-(**1**), Br^-(**2**), NCS^-(**4**), $NCSe^-$(**5**), ClO_4^-(**3,6**). Complexes **1–6** are six-coordinate with the distorted trigonal prismatic geometry imparted by the pentadentate pyridine-/piperazine-based macrocyclic ligand **L** and by one monovalent coligand X^-. Based on magnetic studies, all complexes **1–6** exhibit strong magnetic anisotropy with negative *D*-values ranging from about −20 to −41 cm^{-1}. This variation in *D* (*i.e.* the increase of magnetic anisotropy) parallels the trend obtained by theoretical calculations and the lesser distortion of the coordination sphere with respect to the trigonal prismatic reference geometry. AC magnetic susceptibility investigations revealed field-induced single-molecule magnet behaviour for all complexes except Cl^- derivative **1**. The series investigated represents a rare example of Co(II) complexes with a robust trigonal prismatic geometry.

Introduction

Single-molecule magnets (SMMs)[1,2] are a remarkable class of compounds characterized by slow relaxation of magnetization below the blocking temperature (T_B) of purely molecular origin and exhibiting magnetic bistability like "bulk" magnets. Strong scientific attention has been devoted to SMMs during the last few decades due to their potential relevance in ultra-dense information storage, quantum computing, molecular switches, or spintronics.[1] Magnetization freezing in SMMs is usually related to large axial magnetic anisotropy. In transition metal complexes magnetic anisotropy commonly results from zero-field splitting (ZFS) and is described in spin Hamiltonian formalism by an axial and a rhombic parameter *D* and *E*, respectively.[1] In this formalism, easy-axis anisotropy is characterized by a negative *D* value and easy-plane anisotropy by a positive *D* value. Magnetization blocking can take place for species possessing easy-axis anisotropy. Ideally, magnetization relaxation is expected to be thermally activated and admits an energy barrier defined as $U = |D|S^2$ or $U = |D|(S^2 - \frac{1}{4})$ for the integer or non-integer ground spin state *S*, respectively.[1,2] Species with large and negative *D* values are therefore essential for reaching substantial energy barriers. The higher the *U* value the higher the blocking temperature, which is commonly below ~25 K for molecular complexes except the Dy^{III} metallocene heteroleptic derivative with a record T_B value exceeding the liquid nitrogen temperature (T_B = 80 K, U = 1541 cm^{-1}).[3]

For transition metal ions, the characteristics of magnetic anisotropy for a d^n electronic configuration are directly related to the geometry of their coordination sphere.[4,5] Although remarkable anisotropy has been obtained for low-coordination complexes,[5–7] some of the best SMMs exceeding U = 400 cm^{-1} are extremely unstable[8,9] and hardly suitable to be involved in supramolecular assembly reactions. An alternative is provided by seven-coordinate pentagonal bipyramidal complexes of transition metals.[5,10,11] In this geometry, Fe(II) and Ni(II) complexes possess negative *D*-values and have been involved in the preparation of polynuclear molecular nanomagnets.[11–16] Co(II), with its large orbital angular momentum, revealed substantial but positive *D*-values in this coordination geometry.[17–19] Hence, the design of structurally robust Co(II) complexes with negative *D*-value remains a stimulating but tricky target.

[a]*Department of Inorganic Chemistry, Faculty of Science, Palacký University Olomouc, 17. listopadu 12, 771 46 Olomouc, Czech Republic.*
E-mail: bohuslav.drahos@upol.cz; Fax: +420585 634 954; Tel: +420 585 634 429
[b]*Laboratoire de Chimie de Coordination du CNRS (LCC-CNRS), Université de Toulouse, CNRS, Toulouse, France.*
E-mail: jean-pascal.sutter@lcc-toulouse.fr

†Electronic supplementary information (ESI) available. CCDC 2279916, 2279918, 2279920 and 2279922–2279925. For ESI and crystallographic data in CIF or other electronic format see DOI: https://doi.org/10.1039/d3dt02639f

Six-coordinate Co(II) complexes could be an interesting alternative, not those with the common octahedral geometry, which generally provide positive *D*-values, but rather those with a trigonal prismatic geometry. In this environment Co(II) is expected to exhibit negative *D*-values,[4,5] as was confirmed by previously reported examples including complexes of the Schiff base ligand,[20] clathrochelates,[21–23] or "tripodal-type" ligands[24,25] with *D*-values ranging from −31 cm^{-1} up to −128 cm^{-1} (for more details see Table 4 in the Results and discussion section). However, such compounds remain scarce because it is very difficult to reach a trigonal prismatic coordination geometry which generally results from steric restraints coming from the ligand(s) occupying all coordination sites. We observed that a macrocyclic pentaaza pentadentate ligand, **L** (Fig. 1) led to a trigonal prismatic coordination sphere for transition metals, including Co(II) as illustrated for [Co(**L**)(CH_3CN)][ClO_4]$_2$.[26] We have further studied this trigonal prismatic system and report herein a series of Co(II) complexes based on this ligand in association with a monodentate halido/pseudohalido coligand. Our objective was to evaluate the effect of different ligand field strengths and structural modifications on the magnetic anisotropy of Co(II). Based on magnetic studies, we show that all compounds are characterized by strong axial anisotropy, with *D* values between −20 and −41 cm^{-1}, in agreement with values derived from theoretical calculations. Moreover, SMM-like behaviors have been observed for the majority of the complexes.

Experimental

Materials and methods

All the solvents (VWR International, Fontenay-sous-Blois, France) and other chemicals were purchased from commercial sources (Acros Organics, Geel, Belgium and Sigma-Aldrich, St Louis, MO, USA) and used as received. Silica gel for column chromatography was purchased from Penta, Prague, Czech Republic (Silica gel 100; 0.063–0.2 mm).

A one channel just infusion™ linear pump NE 300 (New Era Pump Systems, Inc., Farmingdale, NY, USA) and an HSW Norm-Ject 20 ml syringe were employed for ligand synthesis (infusion rate 1 mL min^{-1}).

^{1}H and ^{13}C NMR spectra were recorded at the laboratory temperature on a 400 MHz Varian NMR spectrometer for high-resolution solution-state NMR (Varian, Palo Alto, CA, USA): ^{1}H 399.95 MHz, ($CDCl_3$, tetramethylsilane) δ = 0.00 ppm, ^{13}C 100.60 MHz, ($CDCl_3$, residual solvent peak) δ = 77.0 ppm. The multiplicity of the signals was indicated as follows: s – singlet, d – doublet, t – triplet, quin – quintet, and m – multiplet. Deuterated solvent $CDCl_3$, containing 0.03% of TMS, from Sigma Aldrich was used as received. The atom numbering scheme used for NMR data interpretation is shown in Fig. 1.

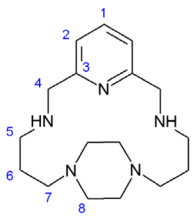

Fig. 1 Structural formula of macrocyclic ligand L together with atom numbering used for NMR assignment.

The mass spectra were collected on an LCQ Fleet mass spectrometer (Thermo Scientific, Waltham, MA, USA) equipped with an electrospray ion source and three-dimensional (3D) ion-trap detector in the positive mode.

IR spectra were recorded on a Jasco FT/IR-4700 spectrometer (Jasco, Easton, MD, USA) using the ATR technique on a diamond plate in the spectral range 4000–400 cm^{-1}.

Elemental analysis (C, H, N) was realized on a Flash 2000 CHNO-S analyzer (Thermo Scientific, Waltham, MA, USA).

Magnetic measurements for all the samples were carried out with a Quantum Design MPMS 5S SQUID magnetometer in the temperature range of 2–300 K. The measurements were performed on polycrystalline samples mixed with grease and put in gelatine capsules. The temperature dependences of the magnetization were measured in an applied field of 1 kOe and the isothermal field dependences of the magnetization were collected up to 5 T at temperatures between 2 and 8 K. The molar susceptibility (χ_M) was corrected for the sample holder, grease and for the diamagnetic contribution of all the atoms using Pascal's tables.[27] AC susceptibility data were collected in the frequency range 1–1500 Hz. Assessment of the ZFS parameters has been done considering an S = 3/2 spin for Co(II), and the software PHI[28] was used for fitting $\chi_M T = f(T)$ and $M = f(H)$ behaviors.

Crystal data refinement

Single crystals of the studied complexes **1–6** suitable for X-ray structure analysis were prepared as described in the Experimental section. The X-ray diffraction data were collected on an XtaLAB Synergy-i (Rigaku, Tokyo, Japan) diffractometer equipped with a HiPix3000 Bantam detector and a monochromatized microfocus PhotonJet-I CuKα radiation source (λ = 1.54184 Å) at room temperature (293(2) K). The molecular structures of studied complexes were solved by direct methods and refined by full matrix least squares based on F^2 (SHELXL 2014/07).[29] Program Olex2 1.3 was used for the final refinement.[30] The hydrogen atoms on carbon atoms were fixed into idealized positions (riding model) and assigned temperature factors either $H_{iso}(H) = 1.2U_{eq}$ (pivot atom) for CH and CH_2 moieties or $H_{iso}(H) = 1.5U_{eq}$ (pivot atom) for CH_3 groups. The molecular and crystal structures of the studied complexes, depicted in Fig. 2 and S3–S9† were drawn using the Mercury software.[31]

Ligand synthesis and characterization

1,5,13,17,22-Pentaazatricyclo[15.2.2.17,11]docosa-7,9,11(22)-triene (**L**). Ligand **L** was prepared according to the modified literature procedure.[26] Pyridine-2,6-dicarbaldehyde (500 mg; 3.7 mmol) and $MnCl_2 \cdot 4H_2O$ (732 mg; 3.7 mmol) were dissolved in methanol (20 mL) and placed in a syringe. 1,4-Bis(3-aminopropyl)

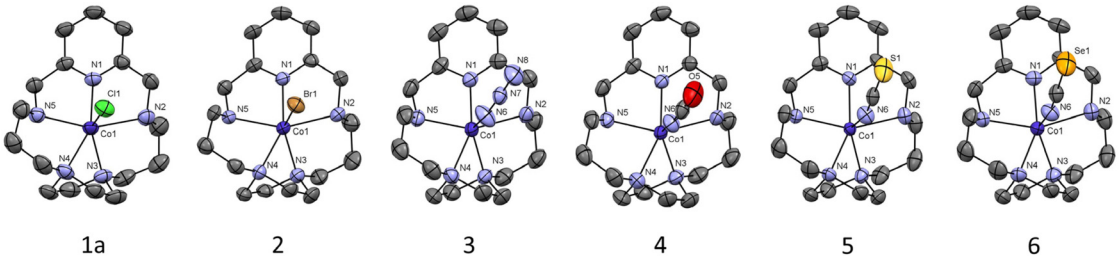

Fig. 2 The molecular structures of the $[CoL(X)]^+$ cations found in the crystal structure of complex **1a** (X = Cl^-), **2** (X = Br^-), **3** (X = N_3^-), **4** (X = NCO^-), **5** (X = NCS^-), **6** (X = $NCSe^-$). Non-hydrogen atoms are drawn as thermal ellipsoids at the 50% probability level. Hydrogen atoms and anions were omitted for clarity. Only one of the two crystallographically independent molecules present in the asymmetric unit of complex **2** is shown for clarity.

piperazine (741 mg; 3.7 mmol) was dissolved in methanol (20 mL) and placed in another syringe. Solutions were added dropwise (infusion rate 1 mL min^{-1}) into stirred methanol (60 mL) in a round bottom flask (250 mL) and the resulting mixture was then refluxed for 2 hours. After cooling down to the laboratory temperature, solid $NaBH_4$ (600 mg; 14.8 mmol) was slowly added portionwise and the reaction mixture was stirred overnight. Distilled water (40 mL) was added, and the suspension was stirred for 1 h. Methanol was removed *in vacuo* and an aqueous solution of NaOH (8 M; 50 ml) was added. The suspension was filtered on a S4 glass frit, and the filtrate was extracted with chloroform (3 × 30 mL). Organic phases were collected, dried with anhydrous $MgSO_4$, filtered on a S4 glass frit and evaporated *in vacuo*. The obtained crude product was purified by silica gel column chromatography using a mixture of ethanol/NH_4OH as a mobile phase (20/1, v/v) and it was obtained in the form of a light brown oil. Yield: 1.021 g; 91%. ^{1}H NMR (400 MHz, $CDCl_3$): δ 7.73 (t, 1H, $^3J_{HH}$ = 7.7 Hz, H1); 7.10 (d, 2H, $^3J_{HH}$ = 7.7 Hz, H2); 3.76 (s, 4H, H4); 3.12 (br. s., 2H, NH); 2.76 (t, 4H, $^3J_{HH}$ = 5.6 Hz, H5); 2.65 (t, $^3J_{HH}$ = 5.6 Hz, 4H, H7); 2.53 (br. s., 8H, H8); 1.68 (quin, $^3J_{HH}$ = 5.6 Hz, 4H, H6). MS *m*/*z* (+): 304.32 (calcd 304.25) [**L**+H]$^+$; 326.30 (calcd 326.23) [**L**+Na]$^+$.

Complex preparation and characterization

Caution! *Perchlorate salts of complexes are hazardous; therefore, heating or scratching them in solid form can lead to explosions.*

Co(II) complexes **1**, **2**, and **5** were prepared in the same way. Equimolar amounts of metal salt (0.330 mmol, *i.e.* 78 mg of $CoCl_2{\cdot}6H_2O$ or 107 mg of $CoBr_2{\cdot}6H_2O$ or 70 mg of Co(SCN)$_2{\cdot}2H_2O$) and ligand **L** (100 mg; 0.330 mmol) were mixed in methanol (4 ml). The complexes were crystallized by vapour diffusion of diethyl ether into the resulting methanolic solution at 7 °C. Complex **1** obtained by the above-mentioned procedure was recrystallized either from methanol/nitromethane (4 ml, 10/1, v/v) or methanol/water/acetone solution (7.5 ml, 2/0.5/5, v/v) by diethyl ether vapour diffusion at 7 °C, yielding single-crystals suitable for X-ray analysis of complex **1a** or **1b**, respectively (crystallization of **1b** was completed within 24 h by standing at 298 K).

Co(II) complexes **3**, **4** and **6** were prepared as follows: Co$(ClO_4)_2{\cdot}6H_2O$ (120 mg; 0.330 mmol) was dissolved in methanol (2 ml) and NaN_3 (86 mg; 1.32 mmol) or NaNCO (86 mg; 1.32 mmol) or KNCSe (190 mg; 1.32 mmol) were added. The solution was filtered and the filtrate was added dropwise to a methanolic solution (2 ml) of **L** (100 mg; 0.330 mmol). The complexes were crystallized as mentioned above.

[CoLCl]Cl·CH$_3$OH·0.5CH$_3$NO$_2$ (1a). Dark blue-green crystals, yield 118 mg (72%). MS *m*/*z*(+): 361.14 (calcd 361.17) [Co**L**−H]$^+$; 397.11 (calcd 397.14) [Co**L**+Cl]$^+$; $C_{18.5}H_{34.5}Cl_2CoN_{5.5}O_2$; M_r = 495.85, found (calcd): C 44.80(44.81); H 7.33(7.01); N 15.14 (15.54); IR (ATR, cm^{-1}): 3191 [ν(N–H)]; 1609, 1590, 1461 [ν(C=C)$_{py}$ + ν(C=N)$_{py}$].

[CoLCl]Cl·3H$_2$O (1b). Dark blue-green crystals, yield 111 mg (69%). MS *m*/*z*(+): 361.13 (calcd 361.17) [Co**L**−H]$^+$; 397.11 (calcd 397.14) [Co**L**+Cl]$^+$; $C_{17}H_{35}Cl_2CoN_5O_3$; M_r = 487.33, found (calcd): C 41.97(41.90); H 7.21(7.24); N 14.37(14.37); IR (ATR, cm^{-1}): 3367 [ν(O–H)]; 3232 [ν(N–H)]; 2856 [ν(C–H)]; 1606, 1581, 1468 [ν(C=C)$_{py}$ + ν(C=N)$_{py}$].

[CoLBr]Br·0.5CH$_3$OH (2). Dark green crystals, yield 119 mg (67%). MS *m*/*z*(+): 361.15 (calcd 361.17) [Co**L**−H]$^+$; 441.10 (calcd 441.09) [Co**L**+Br]$^+$; $C_{17.5}H_{31}Br_2CoN_5O_{0.5}$; M_r = 538.21, found (calcd) C 38.62 (39.05); H 5.74 (5.81); N 12.86 (13.01); IR (ATR, cm^{-1}): 3346, 3176 [ν(N–H)]; 1606, 1585, 1430 [ν(C=C)$_{py}$ + ν(C=N)$_{py}$].

[CoL(N$_3$)]ClO$_4$ (3). Dark green crystals, yield 83 mg (50%). MS *m*/*z*(+): 304.20 (calcd 304.25) [**L**+H]$^+$; 361.11 (calcd 361.17) [Co**L**−H]$^+$; $C_{17}H_{29}ClCoN_8O_4$; M_r = 503.85, found (calcd) C 40.51 (40.52); H 5.71 (5.80); N 22.11 (22.24); IR (ATR, cm^{-1}): 3291 [ν(N–H)]; 2064 [ν(N=N=N)$^-$] 1611, 1588, 1459 [ν(C=C)$_{py}$ + ν(C=N)$_{py}$]; 1084, 620 [ν(ClO$_4$)$^-$].

[CoL(NCO)]ClO$_4$ (4). Dark violet crystals, yield 89 mg (54%). MS *m*/*z*(+): 361.18 (calcd 361.17) [Co**L**−H]$^+$; 404.08 (calcd 404.17) [Co**L**+NCO]$^+$; 461.10 (calcd 461.12) [Co**L**+ClO$_4$]$^+$; $C_{18}H_{29}ClCoN_6O_5$; M_r = 503.85, found (calcd) C 42.78 (42.91); H 5.76 (5.80); N 16.57 (16.68); IR (ATR, cm^{-1}): 3295 [ν(N–H)]; 2210 [ν(N=C=O)$^-$] 1606, 1582, 1463 [ν(C=C)$_{py}$ + ν(C=N)$_{py}$]; 1074, 620 [ν(ClO$_4$)$^-$].

[CoL(SCN)]SCN (5). Purple crystals, yield 142 mg (90%). MS *m*/*z*(+): 304.21 (calcd 304.25) [**L**+H]$^+$; 361.12 (calcd 361.17) [CoLH]$^+$; 420.05 (calcd 420.15) [Co**L**+SCN]$^+$; $C_{19}H_{29}CoN_7S_2$; M_r = 478.54, found (calcd) C 47.68 (47.69); H 6.15 (6.11); N 20.63 (20.49); IR (ATR, cm^{-1}): 3198 [ν(N–H)]; 2083, 2059 [ν(N=C=S)$^-$] 1606, 1582, 1463 [ν(C=C)$_{py}$ + ν(C=N)$_{py}$].

[CoL(SeCN)]SeCN (6). Dark purple crystals, yield 81 mg (43%). MS *m*/*z*(+): 304.20 (calcd 304.25) $[\mathbf{L}+H]^+$; 361.11 (calcd 361.17) $[Co\mathbf{L}-H]^+$; 468.12 (calcd 468.09) $[Co\mathbf{L} + SeCN]^+$; $C_{19}H_{29}CoN_7Se_2$; M_r = 572.33, found (calcd) C 40.18 (39.87); H 4.91 (5.11); N 16.78 (17.13); IR (ATR, cm^{-1}): 3182 [ν(N–H)]; 2082, 2067 [ν(N═C═Se)$^-$] 1605, 1581, 1462 [$\nu(C{=}C)_{py}$ + $\nu(C{=}N)_{py}$].

Computation details

All calculations were performed in the ORCA 5.0.3 software package.[32,33] Computations were performed on complex cations extracted from crystallographic data. First, the positions of hydrogen atoms were optimized by the DFT method using the BP86 functional.[34] Ahlrichs basis set def2-TZVP was chosen for all atoms except for hydrogen and carbon atoms, where a less expensive def2-SVP basis set was employed.[35] Resolution of identity approximation for Coulomb integrals (RI-J)[36] was used together with a def2/J auxiliary basis set[37] in order to speed up calculations. Atom-pairwise dispersion correction based on tight binding partial charges (D4) was also turned on.[38,39]

In order to evaluate magnetic properties, the post-Hartree–Fock method CASSCF(7,5)/NEVPT2 was utilized. The same basis sets were used for geometry optimizations with the addition of def2-TZVP/C as an auxiliary basis set[40] and the chain-of-sphere integration method for Hartree–Fock exchange integrals (COSX).[41] *Ab initio* ligand field orbitals were calculated on molecules oriented according to the *D*-tensors.

Results and discussion

Syntheses and general characterization

The synthesis of the 17-membered macrocyclic ligand **L** was first reported in 2009[42] in 20% yield. In our previous work, we reported that the yield could be increased to about 76% by slow addition of one reagent during the cyclisation step.[26] We further improved the preparation, reaching a yield of 91%, by using two linear pumps to slowly introduce the reagents in the reaction medium. This approach maintained the reagents in a strict stoichiometry at any stage of the cyclo-condensation reaction and ensured high dilution. Thus, a solution of pyridine-2,6-dicarbaldehyde with manganese(II) chloride in 20 mL of methanol in the first syringe and the solution of *N*,*N*′-bis-(3-aminopropyl)piperazine in 20 mL of methanol in the second syringe were added simultaneously to stirred methanol (60 mL) at a continuous infusion rate (1 mL min^{-1}). The subsequent work-up was as previously described.[26] With this modification, we were able to reduce the amount of side products, and significantly increase the yield (up to 91%) of the isolated compound.

Subsequently, a series of six complexes with Co(II) halides and pseudohalides was prepared. Complexes **1a**, **1b**, **2** and **5** were prepared by direct mixing of the Co(II) salt with the ligand in methanol. In the case of complexes **3**, **4** and **6**, the Co(II) salt had to be prepared *in situ* by mixing Co(II) perchlorate with NaN_3, NaNCO or KNCSe, which was then added to the ligand methanolic solution. Except for complexes **1a** and **1b**, which required to be recrystallized from different solvent mixtures, highly crystalline solids were obtained for all complexes directly from the reaction medium. The formation of all complexes was subsequently confirmed by mass spectrometry, elemental analysis, infrared spectroscopy, and single crystal X-ray analysis. It is worth mentioning that no inert conditions were required for the preparation of these complexes and they all are perfectly stable in air in their solid form. This is a quite uncommon feature for Co(II) complexes with pentaaza macrocyclic ligands which usually undergo easy and fast oxidation to Co(III).[43,44]

The measured IR spectra are very similar for all studied complexes. Vibrations corresponding to the macrocycle can be observed in the positions ~3300 cm^{-1} (N–H stretching vibrations); ~1600, ~1500 and ~1460 cm^{-1} (C═C and C═N aromatic vibrations). For complexes **3–6**, stretching vibrations of coordinated anions at 2064 cm^{-1} (–N═N═N), 2210 cm^{-1}, (–N═C═O), ~2080 and ~2060 cm^{-1} (N═C═S; –N═C═Se, two signals due to the presence of one coordinated anion and one non-coordinated counter anion) or those of the perchlorate anion at ~1080 and ~620 cm^{-1} were observed as well.

X-ray diffraction analysis/structural studies

The crystal data and structure refinements are listed in Table 1. The molecular structures of the complex cations of all studied complexes **1a–6** are shown in Fig. 2.

Complexes crystallized in space groups *Pbca* (**1a**, **3**, **4**), *P*$\bar{1}$ (**1b**), *P*2/1*n* (**5**, **6**), and *P*2/1*c* (**2**). All complex cations shown in Fig. 2 have similar structural features. The Co(II) is surrounded by a macrocycle **L** coordinated by all five nitrogen donor atoms and by one monovalent coligand. The coordination sphere for all complexes has distorted trigonal prismatic geometry, which was confirmed by continuous shape measures (deviation between the real and ideal polyhedron geometry) calculated by using the program Shape 2.1 (Table S1†).[45,46] The distortion of the polyhedron increases in order **1a,b** ~ **2** → **5** → **6** → **4** → **3** and it is slightly larger for complexes with pseudohalides (**3–6**) than with halides (**1**, **2**). The coordination bond distances for **1–6** are listed in Table 2 and their comparison is displayed in Fig. 3. Selected bond angles are listed in Table S2.†

It can be noticed that the macrocyclic ligand **L** is significantly twisted. Its shortest coordination bond distances in all complexes are between the central Co(II) atom and the pyridine nitrogen atom N1 with a narrow variation (2.090–2.107 Å) within the series (Fig. 3). The bond lengths between Co(II) and the aliphatic secondary NH groups (N2 and N5) are the same only in **2**, which coordination polyhedron is the closest to the regular trigonal prism. Otherwise, the difference between Co–N2 and Co–N5 distances is about ~0.08 Å, the first being larger than the second, the largest difference is for complexes **3** and **4** (~0.13 Å, Fig. 3). For the coordination bonds involving the piperazine N-atoms, there is also significant difference between them (~0.06 Å), with shorter Co–N3 in comparison with Co–N4 ones, which is rather constant within whole series

Table 1 Crystal data and structure refinements of studied complexes **1–6**

Compound	**1a**	**1b**	**2**	**3**	**4**	**5**	**6**
Formula	$C_{18}H_{33}Cl_2CoN_5O$	$C_{17}H_{35}Cl_2CoN_5O_3$	$C_{35}H_{62}Br_4Co_2N_{10}O$	$C_{17}H_{29}ClCoN_8O_4$	$C_{18}H_{29}ClCoN_6O_5$	$C_{19}H_{29}CoN_7S_2$	$C_{19}H_{29}CoN_7Se_2$
M_r	465.32	487.33	1076.44	503.86	503.85	478.54	572.34
Temperature (K)	293(2)	276(2)	293(2)	293(2)	293(2)	293(2)	293(2)
Wavelength (Å)	1.54184	1.54184	1.54184	1.54184	1.54184	1.54184	1.54184
Crystal system	Orthorhombic	Triclinic	Monoclinic	Orthorhombic	Orthorhombic	Monoclinic	Monoclinic
Space group	*Pbca*	$P\bar{1}$	*P*21/*c*	*Pbca*	*Pbca*	*P*21/*n*	*P*21/*n*
a (Å)	10.7580(2)	8.51040(10)	28.5309(4)	15.3931(2)	15.2438(2)	17.2598(4)	17.3749(2)
b (Å)	13.7934(3)	10.46290(10)	10.45941(15)	16.2764(2)	16.37741(19)	8.01170(10)	8.20480(10)
c (Å)	31.8783(6)	12.91000(10)	14.18701(16)	17.5144(3)	17.6591(2)	17.7444(4)	17.9050(2)
α (°)	90	79.8000(10)	90	90	90	90	90
β (°)	90	81.4420(10)	90.7236(12)	90	90	111.562(2)	111.654(2)
γ (°)	90	88.9580(10)	90	90	90	90	90
V, Å^3	4730.38(16)	1118.75(2)	4233.30(10)	4388.13(11)	4408.67(10)	2281.99(8)	2372.36(6)
Z	8	2	4	8	8	4	4
D_{calc}, g cm^{-3}	1.307	1.447	1.689	1.525	1.518	1.393	1.602
μ, mm^{-1}	7.896	8.439	10.887	7.618	7.591	7.761	9.330
F(000)	1960	514	2176	2104	2104	1004	1148
θ range for data collection (°)	2.772–67.684	3.517–67.684	3.098–67.684	4.691–67.684	4.688–67.684	3.055–67.684	3.029–67.684
Refl. collected	4291	4329	7640	3991	3999	4062	4287
Independent refl.	3456	4141	6033	3343	3261	3490	3873
R(int)[a]	0.0533	0.0311	0.0472	0.0435	0.0356	0.0563	0.0381
Data/restrains/parameters	4291/0/245	4329/3/266	7640/0/471	3991/0/281	3999/0/280	4062/0/262	4287/0/0
Completeness to θ (%)	99.7	99.9	99.1	99.8	99.7	97.6	99.6
Goodness-of-fit on F^2	1.070	1.052	1.147	1.042	1.051	1.054	1.023
R_1, wR_2 ($I > 2\sigma(I)$)[b]	0.0541/0.1579	0.0288/0.0720	0.0662/0.1658	0.0502/0.1459	0.0485/0.1360	0.0529/0.1333	0.0413/0.1075
R_1, wR_2 (all data)[b]	0.0647/0.1661	0.0303/0.0728	0.0856/0.1764	0.0588/0.1531	0.0590/0.1439	0.0604/0.1433	0.0455/0.1102
Largest diff. peak and hole/A^{-3}	0.647/−0.548	0.445/−0.478	1.354/−0.723	0.882/−0.556	0.666/−0.448	0.672/−0.731	1.026/−0.643
CCDC number	2279916	2279918	2279920	2279922	2279923	2279924	2279925

[a] $R_{int} = \sum|F_o^2 - F_{o,mean}^2|/\sum F_o^2$. [b] $R_1 = \sum(||F_o| - |F_c||)/\sum|F_o|$; $wR_2 = [\sum wR_2(F_o - F_o^2)^2/\sum w(F_o^2)^2]^{1/2}$.

Table 2 Selected bond distances (Å) for the studied complexes **1–6**. Two values in the case of complex **2** are given for two crystallographically independent molecules found in the asymmetric unit

	Complex **1a**/**1b**	Complex **2**	Complex **3**	Complex **4**	Complex **5**	Complex **6**
Co–N1	2.097(3)/2.1017(14)	2.109(6) 2.090(6)	2.102(3)	2.107(3)	2.096(3)	2.098(3)
Co–N2	2.306(3)/2.3192(15)	2.274(6) 2.255(7)	2.337(3)	2.346(3)	2.312(3)	2.307(3)
Co–N3	2.209(3)/2.2047(16)	2.197(7) 2.223(7)	2.204(3)	2.209(3)	2.199(3)	2.199(3)
Co–N4	2.257(3)/2.2571(15)	2.254(6) 2.212(7)	2.278(3)	2.281(3)	2.262(3)	2.269(3)
Co–N5	2.241(3)/2.2146(14)	2.256(6) 2.302(7)	2.210(3)	2.213(3)	2.232(2)	2.234(3)
Co–Cl1/Br1/N6	2.4719(9)/2.5082(5)	2.6729(15) 2.6607(15)	2.096(3)	2.059(3)	2.077(3)	2.082(3)

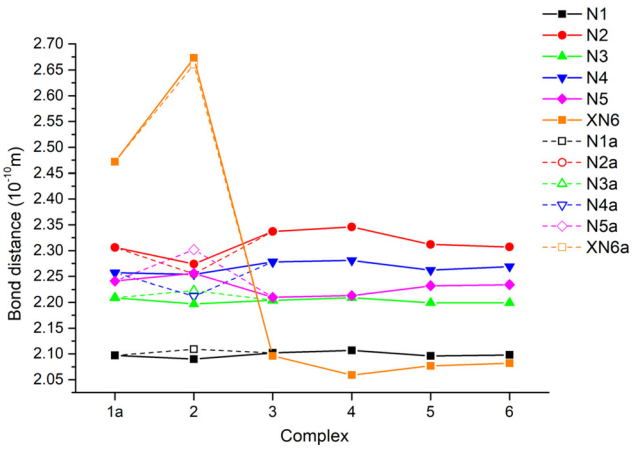

Fig. 3 Comparison of the metal–donor atom distances in complexes **1a–6**. Two values are given in the case of complex **2** for two crystallographically independent molecules found in the asymmetric unit.

(Fig. 3). Thus, three Co–N coordination bonds (N1, N3, N5) are shorter compared to the other two (N2, N4), which confirms the flexibility of the macrocycle.[26] For complexes **1** and **2**, the bond to the halide ligand is rather long (2.472 Å and 2.673/2.661 Å), whereas for complexes **3–6**, the bond with the N-donor coligand atom is 2.059–2.096 Å, shorter than the Co–N1 bond distances.

The two halogenido complexes **1a** and **2** formed supramolecular 1D chains *via* N–H···X hydrogen bonds including the non-coordinated halogenide counter anion (Fig. S3 and S5†). This counter anion forms two N–H···X hydrogen bonds between the secondary amino groups of two macrocyclic units and additionally, forms one hydrogen bond to a co-crystallized CH_3OH solvent molecule. The latter hydrogen bond is present in each 1D chain in complex **1a** while only for one half of the chains in complex **2**. These 1D chains are symmetrically accommodated next to each other along the *b* or *c* axis, respectively (Fig. S3 and S5†), without any non-covalent interaction between each other. On the other hand, complex **1b** formed supramolecular dimers *via* N–H···Cl hydrogen bonds and these dimers are further connected into supramolecular 1D chains by extensive system of N–H···O and O–H···Cl hydrogen bonds. These 1D chains are then connected into a supramolecular 3D network by these extensive O–H···Cl hydrogen bonds as well as π–π stacking interactions (Fig. S4,† $C_g\cdots C_g$ distance is 3.635 Å). The crystal packing of complexes **3** and **4** is very similar to that of previous complexes and again it consists of supramolecular 1D chains *via* N–H···N and N–H···O hydrogen bonds between the first secondary amino group of the macrocycle and coordinated azido or cyanato coligand (Fig. S6 and S7†). These 1D chains are separated by perchlorate anions which are connected *via* N–H···O hydrogen bonds to the second secondary amino group of the macrocycle (Fig. S6 and S7†), but they are not isolated because they are connected to each other *via* π–π stacking interactions ($C_g\cdots C_g$ distance is 3.686 Å (complex **3**) or 3.611 Å (complex **4**)). On the other hand, the crystal packing of complexes **5** and **6** is much more complex. Similar supramolecular 1D chain formation was observed for both complexes (Fig. S8 and S9†), but the geometry of the chains was very different from those in previous complexes. Furthermore $C_{aromatic}$–H···S/Se hydrogen bonds were observed as well as very weak π–π stacking interactions ($C_g\cdots C_g$ distance is 5.532 Å for **5** or 5.512 Å for **6**) which all together form an extensive supramolecular 3D network (Fig. S8 and S9†).

Magnetic properties

All the Co(II) complexes showed very similar $\chi_M T = f(T)$ and $M = f(H)$ behaviours (χ_M stands for the molar magnetic susceptibility), those for $[CoL(N_3)]ClO_4$ (**3**), are plotted as an illustration in Fig. 4; the others are given in the ESI (Fig. S10–S15†). The value found at 300 K for $\chi_M T$ (Table 3) is in agreement with the contribution expected for Co(II) with an $S = 3/2$ ground spin state and $g > 2$ (1.88 $cm^3\ mol^{-1}\ K$ for $g = 2.0$). This value is hardly changed between 300 and about 100 K, then decreases markedly for lower temperatures, a characteristic of a substantial ZFS effect. This effect is also evidenced by the $M = f(H)$ behaviours at 2 K, with a magnetization value for high fields below that of a spin-only behaviour. The characteristic values for each complex are gathered in Table 3. The ZFS parameters were evaluated by analysing these behaviours considering an *S*

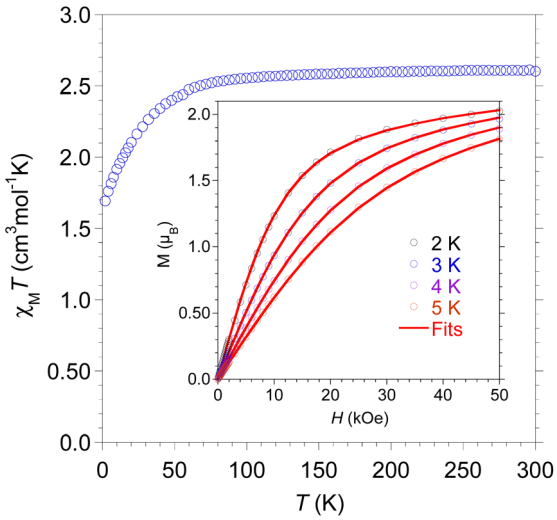

Fig. 4 Temperature dependence of the $\chi_M T$ and the isothermal field dependence of the magnetization (*inset*) for complex **3**. The empty circles are experimental data points, and the full lines represent the best fit with parameter set given in Table 3.

= 3/2 spin. Because the simultaneous analysis of the $\chi_M T = f(T)$ and $M = f(H)$ behaviors with PHI[28] mainly yielded average quality fits, the evaluation of D and E parameters was performed on the magnetization measurements. In all cases, a negative D parameter was obtained with values ranging from −20 to −41 cm^{-1} (Table 3), in agreement with theoretical calculations (*vide infra*). The most negative D value was found for the NCO derivative **4** (−41.2 cm^{-1}) and the less negative for the NCS complex **5** (−19.8 cm^{-1}) suggesting that the variation of the magnetic anisotropy of these complexes is not governed by the ligand field of the coligand ($Br^- < Cl^- < N_3^- < NCO^- < NCS^- < NCSe^-$).[47] But this conclusion must be tempered by the fact that the deformation of the coordination sphere also influences the magnetic anisotropy of each complex.

Further insight was provided by CASSCF/NEVPT2 calculations to obtain ZFS parameters D and E (Table 3). The energy diagrams with the d-orbital splitting, ligand-field terms and ligand-field multiplets are shown in Fig. 5. The splitting of d-orbitals is far from that of an ideal trigonal prismatic ligand field, and the second and third lowest energy orbitals (sharing 3 electrons in the HS d^7 configuration) are no longer degenerate, which is in agreement with rather large distortion of the coordination polyhedron (Table S1†). As a consequence of such lifting of degeneracy, the first-order spin–orbit coupling is not active in **1–6** and the magnetic anisotropy arises only from the second-order spin–orbit coupling, *i.e.* ZFS effect. The calculations also revealed that the change of the coligand X, *i.e.* $Br^- \rightarrow Cl^- \rightarrow N_3^- \rightarrow NCO^- \rightarrow NCS^- \rightarrow NCSe^-$ results in a progressive shift toward higher energy (from about 1000 to 2000 cm^{-1}) of the d-orbital with the 3rd lowest energy (Fig. 5 left), which is directed towards the coligand (see Fig. S16–S23 in the ESI†), thus the separation between the 2nd and 3rd orbitals increases. The above-mentioned trend is in line with the position of the ligands in the spectrochemical series, and follows the increase of the ligand-field strength. As a consequence of such an increase in the energy difference, the splitting of the lowest two LF multiplets decreases (Fig. 5) and thus $|D|$ is reduced in the same order $Br^- \rightarrow Cl^- \rightarrow N_3^- \rightarrow NCY^-$

Table 3 Comparison of *ab initio* calculated and fitted spin Hamiltonian parameters together with magnetization relaxation processes parameters for complexes **1–6**

Compound	**1a** Cl	**1b** Cl	**2** Br	**3** N_3	**4** NCO	**5** NCS	**6** NCSe
				Experimental data			
$\chi_M T$ (cm^3 mol^{-1} K)							
300 K	2.53	3.12	3.04	2.60	2.40	2.70	2.53
2 K	1.72	2.49	1.80	1.69	1.63	1.70	1.50
M (μ_B, 2 K, 5 T)	1.97	2.49	2.29	2.0	1.90	2.27	2.0
				ZFS parameters			
D (cm^{-1})	−36 ± 2	−38.7 ± 0.9	−21.1 ± 0.7	−35.2 ± 0.3	−41.2 ± 0.2	−19.8 ± 0.5	−22.0 ± 0.4
E (cm^{-1})	—	11.3 ± 0.5	3.5 ± 0.5	4.2 ± 0.1	—	5.8 ± 0.5	4.8 ± 0.2
g	2.48	2.85	2.61	2.44	2.38	2.55	2.32
				Magnetization relaxation processes parameters (with respect to eqn (1))			
U/k_B (K)	—	—	—	—	—	32.15 ± 0.08	—
τ_0 (s)	—	—	—	—	—	5.44 ± 0.08 × 10^{-7}	—
R (K^{-n} s^{-1})	—	—	78 ± 365	0.051 ± 0.004	0.015 ± 0.008	—	0. 51 ± 0.02
n	—	—	2.6 ± 2	6.68 ± 0.05	7.4 ± 0.3	—	6.80 ± 0.09
D (K^{-1} s^{-1})	—	—	89 ± 730 × 10^{-6}	5.0 ± 0.7 × 10^{-6}	—	6.7 ± 0.3 × 10^{-6}	1.6 ± 0.2 × 10^{-5}
τ_{QTM} (s)	—	—	0.04 ± 4	—	—	—	—
				ZFS parameters and g values based on CASSCF/NEVPT2 calculations for the first coordination sphere of the complexes			
D (cm^{-1})	−50.1	−48.6	−63.0/−59.6	−37.9	−31.8	−34.5	−33.1
E/D	0.055	0.066	0.053/0.052	0.058	0.057	0.047	0.056
g_x	2.122	2.120	2.095/2.102	2.141	2.151	2.141	2.140
g_y	2.182	2.189	2.170/2.170	2.187	2.190	2.171	2.171
g_z	2.728	2.712	2.849/2.815	2.606	2.544	2.556	2.537
				Calculated g-tensor values of the lowest Kramers doublet with a pseudospin $S = \frac{1}{2}$			
g_x	0.342	0.402	0.326/0.321	0.365	0.357	0.296	0.346
g_y	0.371	0.444	0.356/0.349	0.392	0.381	0.313	0.372
g_z	8.125	8.072	8.466/8.376	7.772	7.592	7.636	7.573

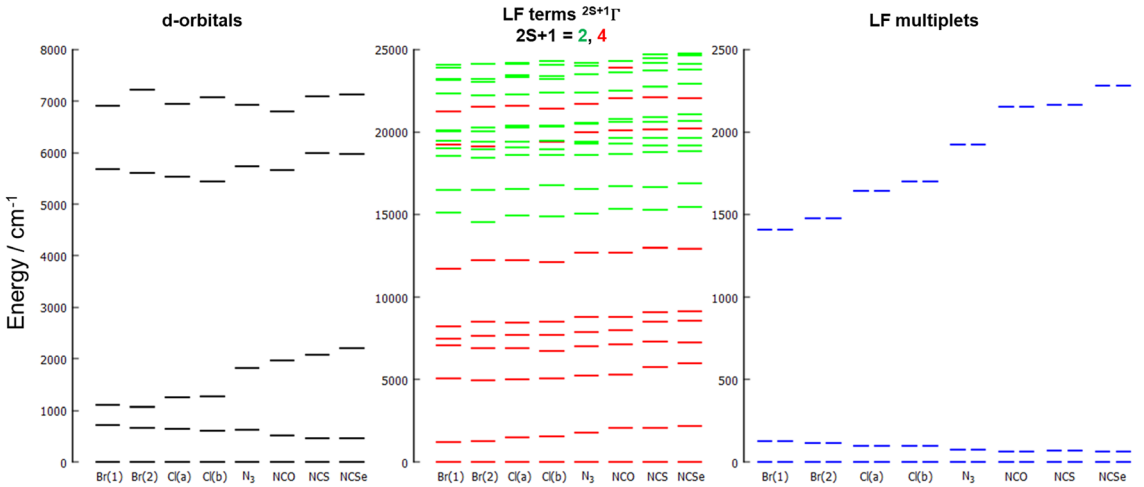

Fig. 5 Results of the CASSCF/NEVPT2 calculations for the studied complexes showing the d-orbital splitting calculated by *ab initio* ligand field theory (AILFT) (left), low-lying ligand-field terms with various multiplicities (middle), and ligand-field multiplets (right).

(Y = O, S, Se), see below for a detailed discussion. Therefore, the largest negative D values can be anticipated for a coligand with the weakest ligand field, typically X = Br^- and Cl^- in the reported series. The contributions to D of the excited states gathered in Table S3 in ESI† confirm that in all cases the largest and negative contribution arises from the mixing with the first excited state. Table S3† also gives the composition of the first two energy states showing their multiconfigurational character without any contribution higher than 60%. This means that any deeper satisfactory analysis (assignment of d-orbitals, evaluation of contributions to D tensor) is difficult in this case.

In general, when the occupation of d-orbitals by 7 electrons (for Co(II)) is considered in an ideal trigonal prismatic ligand field, the transition from the ground to the first exited state is provided by the transfer of one electron between the d_{xy} and $d_{x^2-y^2}$ orbitals (they are sharing 3 electrons). In this process, the magnetic quantum number m_l is not changed, $\Delta m_l = 0$, therefore the contribution to the D-tensor will be large and negative. Thus, in order to better understand the origin of the observed negative D-values and have a comparison with less distorted trigonal prismatic Co(II) systems studied previously, we tried to make an accurate assignment of the d-orbitals obtained by *ab initio* ligand field theory (AILFT) calculations. Therefore, calculations with the molecule oriented according to the D-tensor were taken into account (the principal axes of the D-tensor for each complex are shown in Fig. S16–S23†) and by this approach, the composition of each AILFT d-orbital was obtained (Tables in Fig. S16–S23†). It was therefore possible to correctly assign the AILFT d-orbitals, which proved impossible when a non-oriented molecule was considered. Thus, the d-orbitals with the 2nd and 3rd lowest energy in Fig. 5 left appeared to have mixed contributions from both $d_{x^2-y^2}$ and d_{xy} orbitals. For example, in **1a**, these orbitals contribute 0.42 and 0.32 respectively to the 2nd lowest AILFT d-orbital and 0.44 and 0.50 to the 3rd (see Fig. S16†). Their composition depends on the specific coordinated coligand, but in all cases these two orbitals have the strongest contributions to these AILFT d-orbital (see Fig. S16–S23†). As a result, the coupling of the ground state and the first excited state involves an electron transfer between these two orbitals with $\Delta m_l = 0$ providing a negative and large contribution to D-values (Table S3†). This negative contribution of the 1st excited state is decreasing as the energy separation between the 2nd and 3rd d-orbitals becomes larger, following the trend $Br^- \rightarrow Cl^- \rightarrow N_3^- \rightarrow NCO^- \rightarrow NCS^- \rightarrow NCSe^-$. We have also analysed the contributions to the D-tensor arising from transitions between each electron configuration for the ground and first exited state (see Table S3†). The transitions with $\Delta m_l = 0$ prevail and this is in accordance with the overall large negative contribution of the first exited state to the D-value, which in turn governs the overall D of the compounds.

In order to further confirm the magnetic axiality of the ground Kramers doublet, the g-tensors values for a pseudospin $S = 1/2$ were calculated as well (Table 3). The g-values g_x, $g_y \sim 0$ and $g_z \sim 8$ unambiguously confirmed a highly axial ground Kramers doublet with the Ising-type g-tensor which is in line with the obtained negative D-values and which is comparable[20] with other trigonal prismatic Co(II) complexes with $g_z \sim 9$.[24,25]

The calculated D values appear to be generally overestimated compared to the experimentally obtained ones, but the variation along the series follows the same trend, with the exception of complex **2** with a smaller D value and complex **4** with a rather higher D value. Non-covalent interactions, such as hydrogen bonds, are known to cause such discrepancies, especially when the donor atom of the coordinated ligand is involved. Such hydrogen bonds are indeed found between anion from the outer coordination sphere and the coordinated NH– group of the ligand. We therefore also performed calculations of ZFS parameters with fragments containing uncoordinated anions, these however gave values even further away from those found experimentally.

It is worth noting that ZFS parameters are calculated using spin Hamiltonian which is meaningful only when no low-lying excited state is populated. To reliably describe a system, the norms of its projected states should be closest to 1. Norm values for our complexes are around 0.9 or higher – this from our experience should not cause such a significant deviation as ours but it certainly is a contributing factor. Lastly, the reference structure was obtained at higher temperatures and slight changes in the distortion of the coordination sphere at lower temperature may have an effect on the experimental *D*-value. The aforementioned sources of errors are the most likely reason for the discrepancies.

When the *D* values obtained for **1–6** are compared to those reported for other trigonal prismatic Co(II) complexes (Table 4), they are among the smallest. This appears to correlate with a more distorted trigonal prismatic coordination sphere, and, likely, to the heteroleptic chromophore {CoN_5X}. As discussed above, such a situation leads to a less favourable ligand-field splitting pattern of 3d orbitals and a strongly mixed multiconfiguration composition of wave functions of the ground and low-lying LF states. Thus, the energy separation of d_{xy} and $d_{x^2-y^2}$ orbitals is higher in comparison with other Co(II) complexes in Table 4, which results in lower magnetic anisotropy.[24] Recently, we have observed similar behaviour in a pentagonal bipyramidal system in which a strong distortion of the coordination sphere had a substantial effect on d-orbital splitting and magnetic anisotropy.[48] However, as Table 4 shows, there seems to be no decisive effect of geometry distortion on the *D* values obtained. Some of the most negative values were found for coordination polyhedra that deviate significantly from trigonal prismatic geometry; and *vice versa*. In fact, the magnetic anisotropy of these complexes is directly conditioned by the energy diagram of the d orbitals. In particular, the energy difference between the d_{xy} and $d_{x^2-y^2}$ orbitals is crucial, as it determines whether or not the 1st-order spin–orbit coupling takes place, but also the contribution of ZFS when the degeneracy is lifted. Thus, even when the actual coordination polyhedral deviates from ideal geometry, a rather small energy difference between these orbital results in a large and negative *D*, a situation that applies to $[CoL4]^{2+}$ derivatives[22] mentioned in Table 4. The ligand-field acting on the Co (II) center is directly involved in the d-orbital splitting but its effect in heteroleptic systems is more difficult to apprehend. So, it should be stressed here that the geometry distortion should be related to the *D*-values with great care because the geometry itself does not describe all the aspects of the ligand field (metal–ligand interactions governing the electronic structure of the complex), which is the main driving force for the magnetic anisotropy. On the other hand, the theoretical insights discussed above clearly underline the importance of the coligands interacting with the low-lying d-orbitals.

Table 4 Comparison of the coordination sphere distortion (obtained by continuous shape measures calculations)[a] and *D*-values for complexes **1–6** and reported trigonal prismatic Co(II) complexes

Complex	Deviation for TPR-6	*D*-value (cm^{-1})	Ref.
1a	4.720	−36 ± 2	This work
1b	4.772	−38.7 ± 0.9	This work
2	4.779/4.715	−21.1 ± 0.7	This work
3	5.544	−35.2 ± 0.3	This work
4	5.476	−41.2 ± 0.2	This work
5	5.307	−19.8 ± 0.5	This work
6	5.338	−22.0 ± 0.4	This work
[CoL1]	1.382[a]	−31	20
Clathrochelate 1	0.162[a,b]	−63[b]	21
[CoL2]Cl	0.828[a]	−82	22
$[CoL3](ClO_4)$	0.905[a]	−102.5	23
$[CoL4][CoCl_4]$	3.839	−60.6	24
$[CoL4][ZnCl_4]$	3.196	−87.2	24
$[CoL4](ClO_4)_2$	3.002	−116.6	24
$[CoL4](BF_4)_2$	2.759	−127.6	24
$[CoL5](ClO_4)_2$	0.533	−95.2	25
$[CoL5](BF_4)_2$	0.486	−98.9	25

[a] Calculated using the Shape 2.1 program from the cif file. [b] Values given for the derivative with boron substituent R = F. L1 = piperazine Schiff base, L2 = tris(pyrazoloximate)phenylborate, L3 = tris(methylimidazoloximate)phenylborate, L4 = tris(pyridylhydrazonyl)phosphorylsulfide, and L5 = tris(1-methylimidazolhydrazonyl)phosphorylsulfide.

The possibility that complexes **1–6** exhibit slow relaxation of their magnetization at low temperatures has been explored by AC susceptibility measurements performed in the absence and with an applied static magnetic field. All of them, except for complex **1**, show the appearance of an out of phase component of their susceptibility, χ''_M, in the presence of an applied field (Fig. S10–S15†).

For complex **2**, two relaxation dynamics could be evidenced, suggesting different relaxation characteristics for the two complexes present in the crystal lattice. The observation of the second feature was dependent on the strength of the applied field (Fig. S11†) and the best compromise between strong signal and single (major) relaxation seemed to be for H_{DC} = 1.6 kOe. Therefore, AC data were collected with an applied field of 1.6 kOe. Relaxation time, τ, was obtained from $\chi''_M = f(\nu)$ behaviors (Fig. 6a). The temperature dependence of τ was analysed considering various relaxation mechanisms; in no case it was reproduced by a single model. The Arrhenius law in association with the direct model gave a satisfactory fit but the value for τ_0 was much too large (*ca.* 10^{-5} s), suggesting that relaxation is not thermally activated. Reasonable results have been obtained considering Raman and direct processes with a QTM contribution (respectively the second, third, and fourth terms in eqn (1)). Best fit parameters are gathered in Table 3. Note that the uncertainty on each value is huge.

$$\tau^{-1} = {\tau_0}^{-1} \exp(-U/k_B T) + RT^n + DH^2 T + 1/\tau_{QTM} \quad (1)$$

For azido-complex **3**, the optimal H_{DC} was found to be 2 kOe (Fig. S12†). The frequency dependence of χ''_M obtained in this applied field and the resulting temperature dependence of the relaxation time are plotted Fig. 6b. The variation of τ was best analysed when considering Raman and direct relaxation processes; best-fit parameters are given in Table 3.

For cyanate complex **4**, the longest relaxation time at 2 K was observed for H_{DC} = 1.4 kOe (Fig. S13†) which was con-

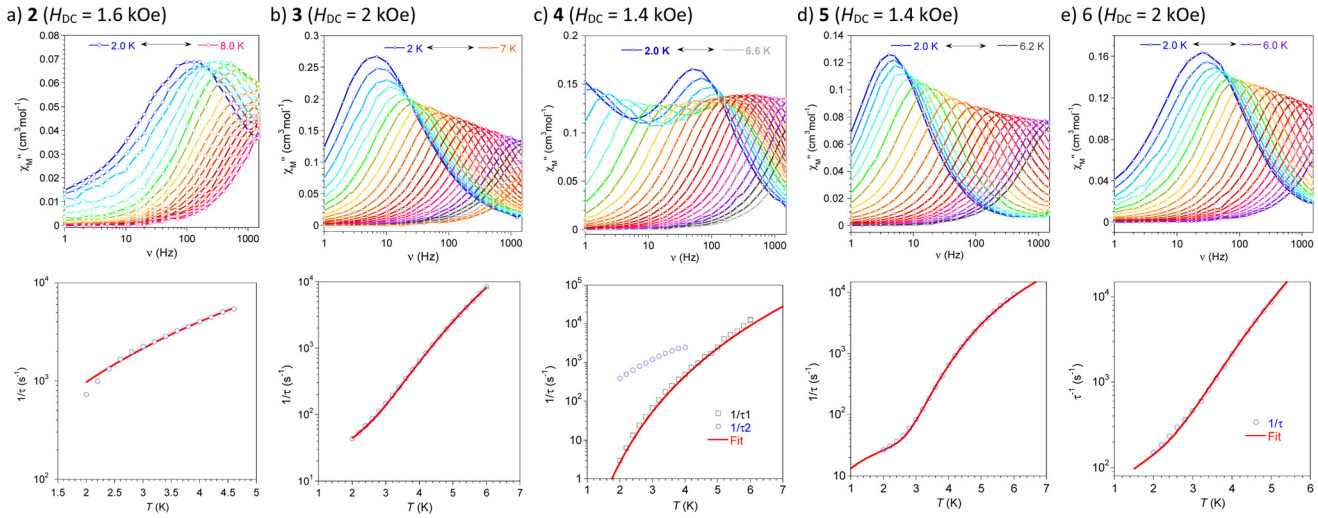

Fig. 6 Frequency dependence of the out-of-phase χ''_M component of AC susceptibility ($\chi''_M = f(\nu)$) for different temperatures (top), and the temperature dependence of the relaxation times ($1/\tau = f(T)$) with calculated behaviour (red lines) for compound **2–6**, respectively, (a)–(e) (bottom).

sidered as the optimal field for subsequent investigations. For this compound, the $\chi''_M = f(\nu)$ behaviors showed two contributions indicative of two distinct dynamics. At low T this gave rise to two well defined maxima, one in the lower frequency range and the second for higher frequencies. Both maxima shift to higher frequencies with increasing temperature, and above 5 K the two contributions merge. The analysis of $\chi''_M = f(\nu)$ was done by a model comprising two extended Debye expressions yielding $\tau 1$ for the signal spanning over the whole frequency domain, and $\tau 2$ for the other (Fig. 6c). These two dynamics are tentatively attributed to a slow relaxation of the magnetization of molecular and lattice origin respectively, for $\tau 1$ and $\tau 2$. The behaviour $1/\tau 1 = f(T)$ could be modelled by a Raman expression (eqn (1)).

For complex **5**, the field dependence studies showed that the signal for χ''_M becomes stronger with the field but that the maximum of $\chi''_M = f(\nu)$ is shifted to larger frequencies (Fig. S14†). Since the high-frequency contribution (attributed to QTM) was suppressed for $H_{DC} > 1.4$ kOe this field was considered the optimal field. The $\chi''_M = f(\nu)$ behaviour obtained by applying this static field and the deduced temperature dependence of τ are depicted in Fig. 6d. The variation of τ was best modelled when contributions from both an Orbach and a direct process were considered (first and third terms in eqn (1)). The linear variation of $\ln(\tau) = f(1/T)$ is characteristic of temperature activated relaxation (Fig. S14†).

For related isoselenocyanate complex, **6**, the signal for χ''_M became stronger with a field of up to 2 kOe and levelled for larger fields (Fig. S15†). The maximum of $\chi''_M = f(\nu)$ did not move with the strength of the applied field; therefore H_{DC} = 2 kOe was chosen for the AC susceptibility studies, the plot of $\chi''_M = f(\nu)$ is given in Fig. 6e. Temperature dependence of the relaxation time could be well modelled when Direct + Raman contributions were considered to take place (Fig. 6e and Table 3).

Conclusions

Efficient and facile access to Co(II) complexes with a trigonal prismatic coordination sphere is made possible by means of pentaaza macrocyclic ligand **L**. The complexes investigated were found to exhibit large magnetic anisotropy characterized by a negative axial ZFS parameter D ranging between −20 and −41 cm^{-1}. These values are less negative than some of the reported trigonal prismatic Co(II) complexes, which may be attributed to more distorted coordination spheres. Theoretical insight revealed d-orbital splitting deviating from the diagram anticipated for a trigonal prismatic geometry and the highly multiconfigurational nature of energy states, which is the main reason for the less negative D-values for all studied complexes. Nevertheless, the origin of magnetic anisotropy is the same as that for other trigonal prismatic Co(II) complexes and relies on the energy difference between d_{xy} and $d_{x^2-y^2}$ orbitals influencing the negative contribution to D from the first exited state. Irrespective of the geometry, the theoretical results show a clear effect of the ligand field strength of the coligand (X). Larger anisotropies, *i.e.* more negative D-values, are achieved for a weaker field X coligand, an important finding for further tuning of the magnetic anisotropy of this system. As a result of such easy-axis magnetic anisotropy all but one of the complexes exhibit field-induced SMM behaviour.

Interestingly, the pentadentate ligand provides the complexes with a robust structural geometry that allows the sixth coordination site to be substituted without compromising the trigonal prismatic coordination polyhedron and thus preserving easy-axis magnetic anisotropy. This feature makes these complexes very interesting units for the design of polynuclear SMMs using the building block/complex-as-ligand approach.

Conflicts of interest

There are no conflicts to declare.

Acknowledgements

The authors gratefully acknowledge the financial support from the Palacký University Olomouc projects IGA_PrF_2021_009 and IGA_PrF_2022_006. The authors are grateful to M. J.-F. Meunier (LCC) for technical assistance in magnetic data collection and to P. Richterová for the measurement of elemental analysis.

References

1 Molecular Nanomagnets and Related Phenomena, in *Structure and Bonding*, ed. S. Gao, Springer, Berlin, 2015, vol. 164.
2 D. Gatteshi, R. Sessoli and J. Villain, *Molecular Nanomagnets*, Oxford University Press, New York, 2006.
3 F.-S. Guo, B. M. Day, Y.-C. Chen, M.-L. Tong, A. Mansikkamäki and R. A. Layfield, Magnetic hysteresis up to 80 kelvin in a dysprosium metallocene single-molecule magnet, *Science*, 2018, **362**, 1400–1403.
4 S. Gómez-Coca, D. Aravena, R. Morales and E. Ruiz, Large magnetic anisotropy in mononuclear metal complexes, *Coord. Chem. Rev.*, 2015, **289–290**, 379–392.
5 A. K. Bar, C. Pichon and J.-P. Sutter, Magnetic anisotropy in two- to eight-coordinated transition–metal complexes: Recent developments in molecular magnetism, *Coord. Chem. Rev.*, 2016, **308**, 346–380.
6 P. P. Samuel, K. C. Mondal, N. Amin Sk, H. W. Roesky, E. Carl, R. Neufeld, D. Stalke, S. Demeshko, F. Meyer, L. Ungur, L. F. Chibotaru, J. Christian, V. Ramachandran, J. van Tol and N. S. Dalal, Electronic Structure and Slow Magnetic Relaxation of Low-Coordinate Cyclic Alkyl(amino) Carbene Stabilized Iron(I) Complexes, *J. Am. Chem. Soc.*, 2014, **136**, 11964–11971.
7 A. Eichhöfer, Y. Lan, V. Mereacre, T. Bodenstein and F. Weigend, Slow Magnetic Relaxation in Trigonal-Planar Mononuclear Fe(II) and Co(II) Bis(trimethylsilyl)amido Complexes—A Comparative Study, *Inorg. Chem.*, 2014, **53**, 1962–1974.
8 X.-N. Yao, J.-Z. Du, Y.-Q. Zhang, X.-B. Leng, M.-W. Yang, S.-D. Jiang, Z.-X. Wang, Z.-W. Ouyang, L. Deng, B.-W. Wang and S. Gao, Two-Coordinate Co(II) Imido Complexes as Outstanding Single-Molecule Magnets, *J. Am. Chem. Soc.*, 2017, **139**, 373–380.
9 P. C. Bunting, M. Atanasov, E. Damgaard-Møller, M. Perfetti, I. Crassee, M. Orlita, J. Overgaard, J. van Slageren, F. Neese and J. R. Long, A linear cobalt(II) complex with maximal orbital angular momentum from a non-Aufbau ground state, *Science*, 2018, **362**, eaat7319.
10 E. L. Gavey and M. Pilkington, Coordination complexes of 15-membered pentadentate aza, oxoaza and thiaaza Schiff base macrocycles "Old Complexes Offer New Attractions", *Coord. Chem. Rev.*, 2015, **296**, 125–152.
11 J.-P. Sutter, V. Béreau, V. Jubault, K. Bretosh, C. Pichon and C. Duhayon, Magnetic anisotropy of transition metal and lanthanide ions in pentagonal bipyramidal geometry, *Chem. Soc. Rev.*, 2022, **51**, 3280–3313.
12 T. S. Venkatakrishnan, S. Sahoo, N. Brefuel, C. Duhayon, C. Paulsen, A. L. Barra, S. Ramasesha and J. P. Sutter, Enhanced Ion Anisotropy by Nonconventional Coordination Geometry: Single-Chain Magnet Behavior for a $[\{Fe^{II}L\}_2\{Nb^{IV}(CN)_8\}]$ Helical Chain Compound Designed with Heptacoordinate Fe^{II}, *J. Am. Chem. Soc.*, 2010, **132**, 6047–6056.
13 Y. Z. Zhang, B. W. Wang, O. Sato and S. Gao, First Fe(II)-based cyano-bridged single molecule magnet $[Cr^{III}Fe^{II}_2]$ with a large anisotropy, *Chem. Commun.*, 2010, **46**, 6959–6961.
14 K. Bretosh, V. Béreau, C. Duhayon, C. Pichon and J.-P. Sutter, A ferromagnetic Ni(II)–Cr(III) single-chain magnet based on pentagonal bipyramidal building units, *Inorg. Chem. Front.*, 2020, **7**, 1503–1511.
15 C. Pichon, N. Suaud, C. Duhayon, N. Guihery and J. P. Sutter, Cyano-Bridged Fe(II)-Cr(III) Single-Chain Magnet Based on Pentagonal Bipyramid Units: On the Added Value of Aligned Axial Anisotropy, *J. Am. Chem. Soc.*, 2018, **140**, 7698–7704.
16 A. K. Bar, N. Gogoi, C. Pichon, V. M. L. D. P. Goli, M. Thlijeni, C. Duhayon, N. Suaud, N. Guihéry, A.-L. Barra, S. Ramasesha and J.-P. Sutter, Pentagonal Bipyramid Fe^{II} Complexes: Robust Ising-Spin Units towards Heteropolynuclear Nanomagnets, *Chem. – Eur. J.*, 2017, **23**, 4380–4396.
17 A. K. Mondal, A. Mondal, B. Dey and S. Konar, Influence of the Coordination Environment on Easy-Plane Magnetic Anisotropy of Pentagonal Bipyramidal Cobalt(II) Complexes, *Inorg. Chem.*, 2018, **57**, 9999–10008.
18 D. Shao, S. L. Zhang, L. Shi, Y. Q. Zhang and X. Y. Wang, Probing the Effect of Axial Ligands on Easy-Plane Anisotropy of Pentagonal-Bipyramidal Cobalt(II) Single-Ion Magnets, *Inorg. Chem.*, 2016, **55**, 10859–10869.
19 B. Drahoš, R. Herchel and Z. Trávníček, Impact of Halogenido Coligands on Magnetic Anisotropy in Seven-Coordinate Co(II) Complexes, *Inorg. Chem.*, 2017, **56**, 5076–5088.
20 Y. Peng, T. Bodenstein, K. Fink, V. Mereacre, C. E. Anson and A. K. Powell, Magnetic anisotropy of a Co^{II} single ion magnet with distorted trigonal prismatic coordination: theory and experiment, *Phys. Chem. Chem. Phys.*, 2016, **18**, 30135–30143.
21 V. V. Novikov, A. A. Pavlov, A. S. Belov, A. V. Vologzhanina, A. Savitsky and Y. Z. Voloshin, Transition ion strikes back: large magnetic susceptibility anisotropy in cobalt(II) clathrochelates, *J. Phys. Chem. Lett.*, 2014, **5**, 3799–3803.
22 V. V. Novikov, A. A. Pavlov, Y. V. Nelyubina, M.-E. Boulon, O. A. Varzatskii, Y. Z. Voloshin and R. E. P. Winpenny, A Trigonal Prismatic Mononuclear Cobalt(II) Complex

Showing Single-Molecule Magnet Behavior, *J. Am. Chem. Soc.*, 2015, **137**, 9792–9795.

23 A. A. Pavlov, D. Y. Aleshin, S. A. Savkina, A. S. Belov, N. N. Efimov, J. Nehrkorn, M. Ozerov, Y. Z. Voloshin, Y. V. Nelyubina and V. V. Novikov, A Trigonal Prismatic Cobalt(II) Complex as a Single Molecule Magnet with a Reduced Contribution from Quantum Tunneling, *ChemPhysChem*, 2019, **20**, 1001–1005.

24 A. Landart-Gereka, M. M. Quesada-Moreno, I. F. Díaz-Ortega, H. Nojiri, M. Ozerov, J. Krzystek, M. A. Palacios and E. Colacio, Large easy-axis magnetic anisotropy in a series of trigonal prismatic mononuclear cobalt(II) complexes with zero-field hidden single-molecule magnet behaviour: the important role of the distortion of the coordination sphere and intermolecular interactions in the slow relaxation, *Inorg. Chem. Front.*, 2022, **9**, 2810–2831.

25 A. Landart-Gereka, M. M. Quesada-Moreno, M. A. Palacios, I. F. Díaz-Ortega, H. Nojiri, M. Ozerov, J. Krzystek and E. Colacio, Pushing up the easy-axis magnetic anisotropy and relaxation times in trigonal prismatic Co^{II} mononuclear SMMs by molecular structure design, *Chem. Commun.*, 2023, **59**, 952–955.

26 E. Zahradníková, R. Herchel, I. Šalitroš, I. Císařová and B. Drahoš, Late first-row transition metal complexes of a 17-membered piperazine-based macrocyclic ligand: structures and magnetism, *Dalton Trans.*, 2020, **49**, 9057–9069.

27 O. Kahn, *Molecular Magnetism*, VCH, Weinheim, 1993.

28 N. F. Chilton, R. P. Anderson, L. D. Turner, A. Soncini and K. S. Murray, PHI: A powerful new program for the analysis of anisotropic monomeric and exchange–coupled polynuclear d– and f–block complexes, *J. Comput. Chem.*, 2013, **34**, 1164–1175.

29 G. M. Sheldrick, Crystal structure refinement with SHELXL, *Acta Crystallogr., Sect. C: Struct. Chem.*, 2015, **71**, 3–8.

30 O. V. Dolomanov, L. J. Bourhis, R. J. Gildea, J. A. K. Howard and H. Puschmann, OLEX2: A complete structure solution, refinement and analysis program, *J. Appl. Crystallogr.*, 2009, **42**, 339–341.

31 C. F. Macrae, I. J. Bruno, J. A. Chisholm, P. R. Edgington, P. McCabe, E. Pidcock, L. Rodriguez-Monge, R. Taylor, J. van de Streek and P. A. Wood, Mercury CSD 2.0 - new features for the visualization and investigation of crystal structures, *J. Appl. Crystallogr.*, 2008, **41**, 466–470.

32 F. Neese, F. Wennmohs, U. Becker and C. Riplinger, The ORCA quantum chemistry program package, *J. Chem. Phys.*, 2020, **152**(22), 224108.

33 F. Neese, Software update: The ORCA program system—Version 5.0., *Wiley Interdiscip. Rev.: Comput. Mol. Sci.*, 2022, **12**, e1606.

34 A. D. Becke, Density-functional exchange-energy approximation with correct asymptotic behaviour, *Phys. Rev. A*, 1988, **38**, 3098–3100.

35 F. Weigend and R. Ahlrichs, Balanced basis sets of split valence, triple zeta valence and quadruple zeta valence quality for H to Rn: Design and assessment of accuracy, *Phys. Chem. Chem. Phys.*, 2005, **7**(18), 1463–9076.

36 F. Neese, An improvement of the resolution of the identity approximation for the formation of the Coulomb matrix, *J. Comput. Chem.*, 2003, **24**(14), 1740–1747.

37 F. Weigend, Accurate Coulomb-fitting basis sets for H to Rn, *Phys. Chem. Chem. Phys.*, 2006, **8**(9), 1057–1065.

38 E. Caldeweyher, C. Bannwarth and S. Grimme, Extension of the D3 dispersion coefficient model, *J. Chem. Phys.*, 2017, **147**(3), 034112.

39 E. Caldeweyher, S. Ehlert, A. Hansen, H. Neugebauer, S. Spicher, C. Bannwarth and S. Grimme, A generally applicable atomic-charge dependent London dispersion correction, *J. Chem. Phys.*, 2019, **150**(15), 154122.

40 A. Hellweg, C. Hättig, S. Höfener and W. Klopper, Optimized accurate auxiliary basis sets for RI-MP2 and RI-CC2 calculations for the atoms Rb to Rn, *Theor. Chem. Acc.*, 2007, **117**(4), 587–597.

41 F. Neese, F. Wennmohs, A. Hansen and U. Becker, Efficient, approximate and parallel Hartree–Fock and hybrid DFT calculations. A 'chain-of-spheres' algorithm for the Hartree–Fock exchange, *Chem. Phys.*, 2009, **356**(1–3), 98–109.

42 H. Keypour, M. Rezaeivala, L. Valencia and P. Pérez-Lourido, Synthesis and characterization of some new Pb(II), Mn(II) and Ag(I) complexes with a pentaaza macrocyclic ligand containing a piperazine moiety, *Polyhedron*, 2009, **28**(18), 4096–4100.

43 M. C. Rakowski, M. Rycheck and D. H. Busch, Synthesis and Characterization of Transition Metal Complexes Containing a Pentadentate Macrocyclic Ligand, *Inorg. Chem.*, 1975, **14**, 1194–1200.

44 B. Drahoš, J. Kotek, P. Hermann, I. Lukeš and E. Tóth, Mn^{2+} Complexes with Pyridine-Containing 15-Membered Macrocycles: Thermodynamic, Kinetic, Crystallographic, and $^{1}H/^{17}O$ Relaxation Studies, *Inorg. Chem.*, 2010, **49**, 3224–3238.

45 D. Casanova, P. Alemany, J. M. Bofill and S. Alvarez, Shape and Symmetry of Heptacoordinate Transition-Metal Complexes: Structural Trends, *Chem. – Eur. J.*, 2003, **9**, 1281–1295.

46 S. Alvarez, Polyhedra in (inorganic) chemistry, *Dalton Trans.*, 2005, 2209–2233.

47 I. Nemec, R. Herchel, R. Boča, Z. Trávníček, I. Svoboda, H. Fuess and W. Linert, Tuning of spin crossover behaviour in iron(III) complexes involving pentadentate Schiff bases and pseudohalides, *Dalton Trans.*, 2011, **40**, 10090–10099.

48 B. Drahoš and R. Herchel, Effective tuning of magnetic anisotropy in distorted pentagonal bipyramidal Ni(II) complexes via substitution of axial coligands, *Dalton Trans.*, 2022, **51**, 18033–18044.